Journal Pre-proof

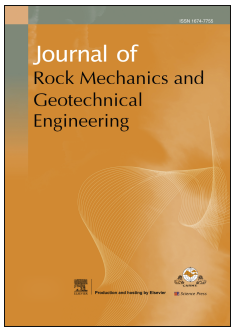

Post-liquefaction shearing behaviour of saturated gravelly soils: Experimental study and discrete element simulation

Yong Wang, Yanli Wang, Lingwei Kong, Zhiliang Sun

PII: S1674-7755(20)30091-3

DOI: https://doi.org/10.1016/j.jrmge.2020.01.007

Reference: JRMGE 685

To appear in: *Journal of Rock Mechanics and Geotechnical Engineering*

Received Date: 23 July 2019

Revised Date: 23 November 2019

Accepted Date: 12 January 2020

Please cite this article as: Wang Y, Wang Y, Kong L, Sun Z, Post-liquefaction shearing behaviour of saturated gravelly soils: Experimental study and discrete element simulation, *Journal of Rock Mechanics and Geotechnical Engineering*, https://doi.org/10.1016/j.jrmge.2020.01.007.

Journal Pre-proof

Journal of Rock Mechanics and Geotechnical Engineering

Journal online: www.rockgeotech.org

Technical Note

Post-liquefaction shearing behaviour of saturated gravelly soils: Experimental study and discrete element simulation

Yong Wang [a,*], Yanli Wang [b], Lingwei Kong [a], Zhiliang Sun [a]

[a] *State Key Laboratory of Geomechanics and Geotechnical Engineering, Institute of Rock and Soil Mechanics, Chinese Academy of Sciences, Wuhan, 430071, China*

[b] *Yangtze River Scientific Research Institute, Key Laboratory of Geotechnical Mechanics and Engineering of the Ministry of Water Resources, Wuhan, 430010, China*

Received 23 July 2019; received in revised form 23 November 2019; accepted 12 January 2020

Abstract: To investigate the post-liquefaction shearing behaviour of saturated gravelly soil, laboratory tests were conducted using a static-dynamic multi-purpose triaxial apparatus. In addition, numerical simulations using the discrete element method (DEM) were performed to preliminarily understand the micro-mechanism of gravelly soil in monotonic loading after liquefaction. The influences of dry density, initial confining stress and degree of liquefaction on the post-liquefaction shearing behaviour of gravelly soil were discussed, and the evolution of the micro-parameters of the granular system was also analysed. The results show that the stress-strain responses of gravelly soil after liquefaction can be divided into three stages: (1) low strength stage, (2) super-linear strength recovery stage, and (3) sublinear strength recovery stage, which are distinctly different from those of the general saturated gravelly soil without previous cyclic loading. The initial state and prior dynamic stress history have significant influences on the post-liquefaction shearing behaviour of gravelly soil. The DEM simulation revealed that the average coordination number sharply increases, the contact normal shows an obvious orientation distribution, and the destroyed force chain backbones are reconstructed in the monotonic reloading process after liquefaction. The evolution of the micro-parameters of the granular system clearly reflects the interior interaction process and micro-mechanisms in the particles during the three different stages of the macro-mechanical behaviour of gravelly soil.

Keywords: post-liquefaction; micro-mechanism; gravelly soil; deformation; discrete element method (DEM)

1. Introduction

Gravelly soils are frequently encountered in natural soil strata, such as residual, fluvial, alluvial, and glacial deposits, as well as artificial fills (embankments and reclaimed gravelly fills) (Chang et al., 2014). Due to their coarse particles and good permeability, they are frequently mistakenly regarded as non-liquefiable (Chen et al., 2009; Cao et al., 2011). However, liquefaction scenarios of gravelly soil have been observed in several earthquakes, e.g. the Hokkaido-Nansei-Oki earthquake in 1993 (Kokusho et al., 1995) and the M_s 8.0 Wenchuan earthquake in 2008 (Cao et al., 2010). Some laboratory tests also showed the liquefaction possibility of gravelly soil. Wong et al. (1975) and Baneriee et al. (1979) performed a series of undrained cyclic triaxial tests and found that gravel soil has an "initial liquefaction" phenomenon. Evans and Zhou (1995) studied the influence of gravel content on the liquefaction of gravelly soil and concluded that the liquefaction resistance increases with increasing gravel content under the same relative density. Kokusho et al. (2004) revealed that the undrained cyclic strength of gravelly soil mainly depends on the relative density rather than particle gradations. Based on the field reconnaissance in Wenchuan earthquake, Hou et al. (2011) found that the gravel content and the relative density have sound effects on the liquefaction resistance of sand-gravel soils. Due the typical multi-scale structure of gravelly soil, Wang and Wang (2017a,b) used computed tomography (CT) scanning tests and numerical simulations by the discrete element method (DEM) to investigate the influence of gravel content and liquefaction micro-mechanism of gravelly soil, respectively. In addition, over the last decade, several methods for liquefaction discrimination of gravelly soil have also been proposed (Lin et al., 2004; Cao et al., 2013). In short, more evidences confirm the liquefiable feature of gravelly soil, and the understanding of their liquefaction should be deepened from the general macroscopic phenomenon and resistance strength to microscopic mechanisms and liquefaction discrimination.

In fact, the widespread liquefaction-induced damages to soils and foundations are composed of residual deformation generated under cyclic loads during earthquakes and resultant deformation generated by gravity (i.e. post-liquefaction deformation) (Wang et al., 2013). The displacements induced by post-liquefaction deformation of soil after earthquake can be large enough to produce severe damage to earth structures, including dams and embankments (Tohno and Shamoto, 1985; Hamada and Rourke, 1992; Yoshida et al., 1992; Tokimatsu et al., 1994; Cubrinovski et al., 2012; Yasuda et al., 2012; Ishikawa et al., 2015). In recent years, several researchers have investigated the post-liquefaction behaviour of gravelly soil. For example, Xu et al. (2007) proposed a trilinear model based on laboratory tests to describe the post-liquefaction deformation of sand-gravel composites. Pan et al. (2012) performed hollow cylinder tests on the saturated sand-gravel composites after liquefaction to investigate the characteristics of the stress−strain relationship and the dissipation of pore water pressure. However, these studies mainly focused on the macroscopic post-liquefaction deformation

*Corresponding author. E-mail address: wang831yong@126.com

behaviour of gravelly soil, but few were concerned with a microscopic perspective.

In this work, we aimed to investigate the post-liquefaction shearing behaviour and microscopic evolution mechanism of gravelly soil. Monotonic loading tests were conducted on saturated gravelly soil after liquefaction using a dynamic-static triaxial system, Geotechnical Digital Systems (GDS). The strength, stress-strain behaviour and pore water pressure of saturated gravelly soil in monotonic reloading were investigated. Next, the effects of dry density, confining stress and degree of liquefaction on its undrained shearing characteristics were analysed. Finally, DEM simulations of the post-liquefaction shearing behaviour of saturated gravelly soil were performed using the particle flow code (PFC) to reveal the intrinsic micro-mechanisms and evolution features.

2. Experimental procedure and results

2.1. Sample preparation

Gravelly soil specimens with grain sizes no larger than 20 mm were collected from a dam site of the Xiang River water conservancy hub, Tibet, China. The dried soil specimens were successively sieved with 20 mm, 10 mm, 5 mm, 2 mm, and 0.075 mm screens, as shown in Fig. 1a. The particles with sizes of 2-20 mm were selected as gravel and those less than 2 mm were considered as sand. The GDS dynamic-static triaxial tests were conducted on isotropically consolidated specimens with dimensions of 101 mm (diameter) × 200 mm (height) under undrained conditions (Fig. 1b). The grain size distribution of the soil specimens is shown in Fig. 2. To obtain the indices e_{max} and e_{min} of gravelly soil (e_{max} and e_{min} are the maximum and minimum void ratios, respectively), tests on the specific gravity G_s and relative density D_r were firstly conducted. Then, the minimum dry density ρ_{dmin} was determined using a fixed volume method (test tube ⌀300 mm × 360 mm), and the maximum dry density ρ_{dmax} was determined using the surface vibration method at frequency of 50 Hz (Wang and Wang, 2017a). Thus, the associated indices are obtained as G_s = 2.753, e_{max} = 0.72, and e_{min} = 0.336.

(a)

(b)

Fig. 1. The tested specimens and apparatus. (a) The screened test soil specimens; and (b) The GDS dynamic-static triaxial system.

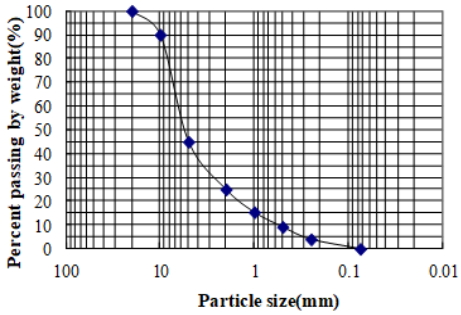

Fig. 2. Grain size distribution of the tested specimens.

The remoulded specimens were composed of four layers, which were prepared using the multi-level wet pounding method. Based on the dry density and moisture content of the soil specimens, each layer with the same weight was compacted to a height of 50 mm. The interface was scarified to ensure close contact between the layers.

2.2. Test procedure

The prepared specimens were fully saturated with de-aired water using a combination of hydraulic saturation method and back-pressure saturation method. The specimens were flushed with de-aired water from bottom to top for 12 h, while they were subjected to an effective confining stress of approximately 20-30 kPa. Each specimen was saturated with back-pressure incrementally up to 200 kPa until the *B*-value was larger than 0.95, where $B = \Delta u/\Delta\sigma_3$, in which $\Delta\sigma_3$ is the increase of confining stress applied to the specimen, and Δu is the resulting change in pore water pressure. The specimens were isotropically consolidated under a given initial effective confining stress σ_{3c}. The isotropic consolidation stability was considered to be achieved when the volumetric change of the specimens remained unchanged in 5 min. Undrained stress-controlled sinusoidal cyclic loading (cyclic stress ratio, $\sigma_d/(2\sigma_c') = 0.25$, where σ_d is the single axial stress amplitude and σ_c' is the effective confining stress) with a frequency of 0.2 Hz was then applied until "initial liquefaction" occurred, which is defined as the pore water pressure being equal to the confining stress (Seed and Lee, 1966). After initial liquefaction, a strain-controlled monotonic load was applied under undrained conditions to analyse the post-liquefaction shearing behaviour of the gravelly soil. The monotonic load was applied at a rate of 0.5 mm/min. The loading process is shown in Fig. 3. The axial load, cell pressure, pore water pressure, and axial displacement were recorded in real time

during the cyclic and monotonic loading. Before the monotonic loading test, the typical curves of the specimens (σ_c' = 300 kPa) during the cyclic loading are shown in Fig. 4.

Soil liquefaction can basically be divided into local liquefaction and complete liquefaction in field. Local liquefaction occurs first, and then the liquefied area gradually expands. Thus, a site could experience different degrees of liquefaction during earthquake. The post-liquefaction responses of gravelly soils could be affected by different degrees of liquefaction. Fukutake et al. (1990) proposed a concept of a liquefaction safety ratio (F_l) to reflect the severity of liquefaction based on the Seed–Idriss method. It was defined as the ratio between the actual dynamic stress of the soil and the peak stress under seismic loading. However, Yasuda et al. (1995) found that different cyclic numbers with same dynamic stress also have a significant effect on the static stress-strain relationship of the saturated soil after liquefaction. For easy control, they proposed another method to define F_l as the severity of liquefaction based on the vibration cycles:

$$F_l = \frac{n}{m} \tag{1}$$

where n is the number of vibration cycles achieving the initial liquefaction of the specimens under a given cyclic shear stress ratio, and m is the actual number of vibration cycles under the same cyclic shear stress ratio during the test. In this work, the conception of F_l was used to reflect different degrees of liquefaction with the same definition proposed by Yasuda et al. (1995).

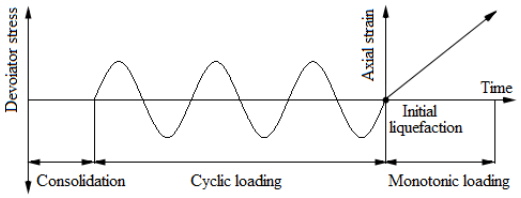

Fig. 3. The loading process of the post-liquefaction test.

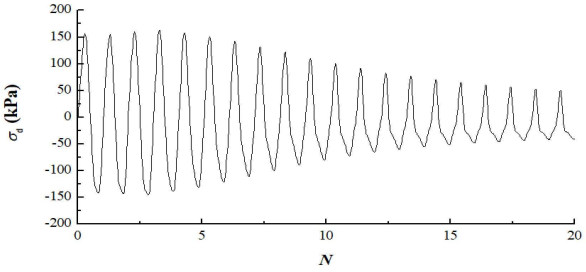

(a)

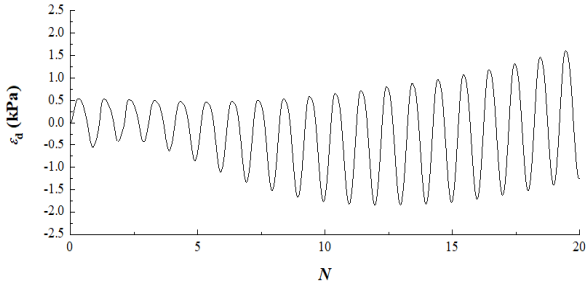

(b)

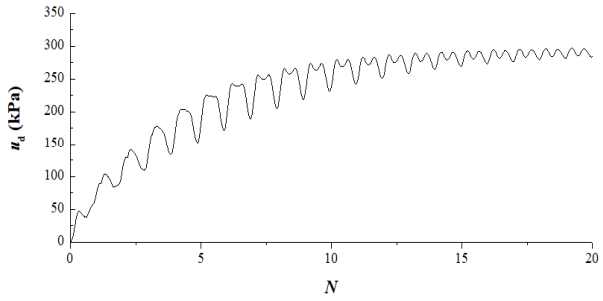

(c)

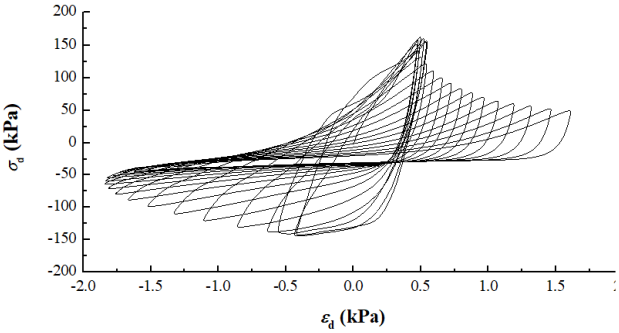

(d)

Fig. 4. Typical curves of the specimens during cyclic loading (σ_c' = 300 kPa). Variation in (a) dynamic axial stress σ_d with the number of loading cycles N; (b) dynamic axial strain ε_d with the number of loading cycles N; (c) dynamic excess pore water pressure u_d with the number of loading cycles N; and (d) dynamic axial stress σ_d with the dynamic axial strain ε_d.

Fig. 5 shows the schematic of dynamic loading curve. It can be seen that when $F_l = 1$, the soil specimens reach the initial liquefaction point; when $F_l > 1$, the soil specimens have not reached the initial liquefaction; and when $F_l < 1$, the soil specimens have reached the initial liquefaction point, but the cyclic loading continues to act for a certain period of time. A lower value of F_l indicates a greater degree of liquefaction.

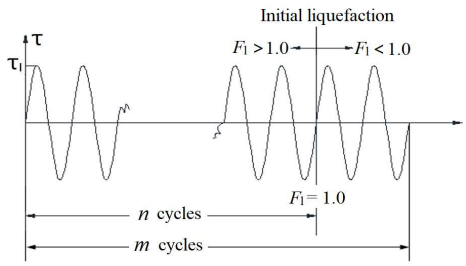

Fig. 5. Schematic of different degrees of liquefaction.

This study investigated the influences of initial dry density (ρ_d), initial effective confining stress (σ_{3c}) and F_l on the post-liquefaction shearing behaviour of saturated gravelly soil. The following parameters are obtained: ρ_d = 1.7 g/cm^3, 1.8 g/cm^3, and 1.9 g/cm^3; σ_{3c} = 100 kPa, 200 kPa, and 300 kPa; and F_l = 0.8, 0.9, 1.0, 1.2, and 1.5. The test scheme of gravelly soil is listed in Table 1. In the tests, the effect of membrane penetration is approximately taken into consideration by employing the modification method originally proposed by Tokimatsu and Nakamura (1987) and modified by Tanaka et al. (1991).

Table 1.

Test scheme of gravelly soil after liquefaction.

Dry density, ρ_d (g/cm^3)	The relative density, D_r	Water content, w (%)	Initial effective confining stress, σ_{3c}(kPa)	Degree of liquefaction, F_l
1.7	0.3	22.5	100	1
1.8	0.5	19.2	100	0.8
				0.9
				1
				1.2
				1.5
			200	1
			300	1
1.9	0.7	16.3	100	1

2.3. Test results and analysis

2.3.1. The macro-mechanical responses

Fig. 6 shows a comparison of shearing behaviour in the monotonic shearing test between the typical specimen after liquefaction and corresponding saturated specimen without prior cyclic loading (ρ_d = 1.8 g/cm^3, σ_{3c} = 100 kPa). The stress-strain relationship of the liquefied specimen is significantly different from that of the ordinary saturated specimen. The results show that the liquefied gravelly soil specimen initially shows a low stiffness within a small range of axial strain. Subsequently, the stiffness of the soil specimen begins to recover rapidly. The deviatoric stress q shows an S-shape variation with the axial strain ε_a (the line with black square marks), but the excess pore water pressure u presents a reverse S-shape curve (the line with red dots). Furthermore, the ultimate strength of the liquefied specimen is much larger than that without prior cyclic loading, and the change in pore water pressure is more dramatic under the same conditions. The stress-strain behaviour of the liquefied specimens can be divided into three stages, i.e. low strength stage, super-linear strength recovery stage, and sublinear strength recovery stage, while the specimen without cyclic loading experiences only one stage. As shown in Fig. 6, $L(\varepsilon_{d0}, q_0)$ on the stress-strain curve of the liquefied specimen is defined as the demarcation point between the first and the second stage, which corresponds to the axial strain ε_{d0}. After point L, the tangent modulus of the liquefied gravelly soils begins to increase quickly, and the accumulated excess pore water pressure u_d during the cyclic loading begins to decrease instead of remaining constant as the effective confining pressure. Point N corresponds to the peak strength of the stress-strain curve at an allowable ultimate strain (e.g. 15%). Point $M(\varepsilon_{d1}, q_1)$ is defined as the demarcation point between the second and the third stage, at which the corresponding axial strain is ε_{d1}. The shape of the stress-strain curve, appearing as concave upward before point M, turns into convex upward after point M. In other words, the dependency of the soil stiffness on shear stress is shown obeying from super-linear to sublinear rule. Point M can be roughly determined by the intersection between the straight line LN and the stress-strain curve of gravelly soil after liquefaction.

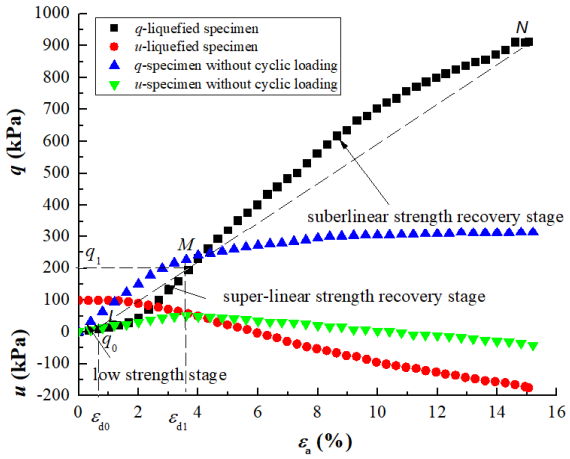

Fig. 6. The typical three stages of post-liquefaction shearing behaviour of gravelly soil specimens.

(1) The first stage (the low strength stage)

The first stage is the initial phase of the post-liquefaction shearing behaviour of gravelly soils. At this stage, the deviatoric stress remains nearly zero ($q \leq 10$ kPa), but the axial strain ε_a increases quickly ($\varepsilon_a \leq 1\%$). The tangent modulus of the soil increases from 0 to a minimal value, and the pore water pressure u remains nearly constant as the confining pressure (the effective stress $\approx$ 0). Therefore, the soil behaviour at this stage appears to be similar to that of a fluid bearing no or very low shear resistance, which is called the low strength stage defined by Shamoto et al. (1997). Under the undrained condition, the specimen has a trend of vibro-contraction under the previous cyclic loading, and the accumulated u of the soil cannot dissipate, during which time the pore water is in a volume-contraction status. Under subsequent static reloading, a trend of shear dilation occurs in the soil, resulting in transformation of the pore water from the contraction to free status, and the external load transferring the stress borne by the pore water to the soil skeleton. With an increasing effective stress, the resistance of the liquefied gravelly soil begins to recover. Usually, gravelly soil has a stronger dilatancy due to the nature of relatively coarser grains and heavier particle systems. This means that the strength of gravelly soil can be recovered after liquefaction in a relatively short period of time.

(2) The second stage (the super-linear strength recovery stage)

After point L, the shearing behaviour of gravelly soil comes into the second stage. At this stage, the pore water of the specimen transforms to a free state wholly as the axial strain develops. The excess pore water pressure accumulated under cyclic loading decreases

sharply, and the effective stress of the soil increases rapidly. This leads to rapid increases in the tangent modulus and sharp recovery of the strength of the gravelly soil. This stage is called the super-linear strength recovery stage. It is worth noting that the developed strain at this stage ($\Delta\varepsilon_a = \varepsilon_{d1}-\varepsilon_{d0}$) is greater than that in the low strength stage, but it is still not large for gravelly soil ($\varepsilon_{d1} \leq 4\%$). Furthermore, the accelerated reduction in pore water pressure at this stage means that a stronger dilatancy trend is generated due to the interior gravel particle rearrangement of the specimen within the limited macro-strain development.

(3) The third stage (the sublinear strength recovery stage)

After point *M*, the shearing behaviour of the gravelly soil is different from those at former two stages, and the stress-strain relationship curve appears as convex upward. At this stage, the specimen is still under the state of shear dilation, and the deviatoric stress increases continuously while the tangent modulus decreases. However, the trend of deviatoric stress grows slowly with increasing axial strain. Meanwhile, the reduction rate of the pore water pressure is also smaller than that at the second stage. This indicates that the dilatancy trend of the gravelly soil begins to weaken, suggesting the gradual stabilization of the particle skeleton adjustment. This stage is called the sublinear strength recovery stage. Because of the limit of the allowable ultimate strain (e.g. 15%), the monotonic tests of the gravelly soil were terminate forcedly, resulting in no horizontal line of the stress-strain curve for the liquefied specimen at the end of the tests compared to that without cyclic loading (Fig. 6). However, with the help of test data, it can be found that there is such a trend. Additionally, the negative excess pore water pressure has been accumulated gradually at this stage, which results in a higher ultimate strength than that of the specimen without cyclic loading.

2.3.2. Investigations of influential factors

(1) The initial dry density

Fig. 7 shows the post-liquefaction responses of gravelly soils with different initial dry densities at the same initial effective confining stress (σ_{3c} = 100 kPa) in terms of variations in the deviatoric stress and excess pore water pressure with the axial strain. As shown in Fig. 7a, the initial dry density significantly affects the post-liquefaction stress-strain behaviour of the gravelly soil. The higher the initial dry density is, the stronger the dilatation trend becomes, resulting in shorter low strength stage and faster recovery of shear capacity. In Fig. 7b, there is a correspondence between the excess pore pressure curves and stress-strain curves. The inflection points of the stress-strain curves clearly correspond to those of the excess pore pressure dissipation curves. Moreover, the initial dry density has a significant influence on the development of the pore water pressure of the gravelly soil at the post-liquefaction stages. The decrease rates of pore pressure of the dense specimens are different from those of the specimens with lower initial dry densities; the pore pressures of the gravelly soils with higher initial dry densities decrease more rapidly, and the strengths recover more quickly. This shows that a larger initial dry density leads to a stronger tendency of dilatancy for the post-liquefaction shearing behaviour of gravelly soil.

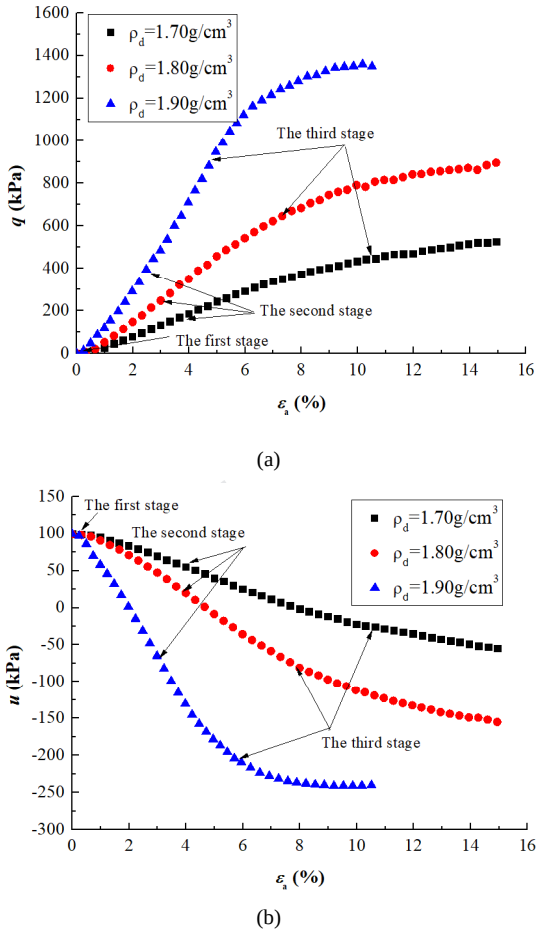

Fig. 7. Post-liquefaction response of the gravelly soil with different initial dry densities. Variation in (a) deviatoric stress *q*; and (b) excess pore water pressure *u* with axial strain ε_a.

(2) The initial effective confining stress

Fig. 8 shows the post-liquefaction responses of gravelly soils with different initial effective confining stresses at the same initial dry density (ρ_d = 1.8 g/cm^3) in terms of the variations in the deviatoric stress and excess pore water pressure with axial strain. The results show that the initial effective confining stress influences the post-liquefaction shearing behaviour of the gravelly soil. This indicates that the behaviour of granular soil essentially depends on its initial state (Been and Jefferies, 1985). As shown in Fig. 8, the larger the initial effective confining stress, the longer the low strength stage, and the higher the late strength. Moreover, it is interesting that the dissipation rates of excess pore water pressure for the specimens with different initial effective stresses are almost parallel at the first and second stages. Only at the third stage, they begin to show differences. Because the number of cycles leading to initial liquefaction for the specimen with higher initial effective stress is larger than that with lower initial effective stress under the same cyclic dynamic stress, the specimen with higher effective stress accumulates a stronger tendency of volume reduction. Therefore, the transformation process in which the pore water is released from the initial compression state to be free is slower than that of the specimens with relatively lower effective confining stress. This is the reason that specimens with larger effective confining stress have a longer low strength stage. However, at the sublinear strength recovery stage, the faster accumulation of negative excess pore pressure caused by stronger dilatancy impedes the weakening of the shear stiffness,

leading to a higher ultimate strength under the permission of sufficiently large macro-strain.

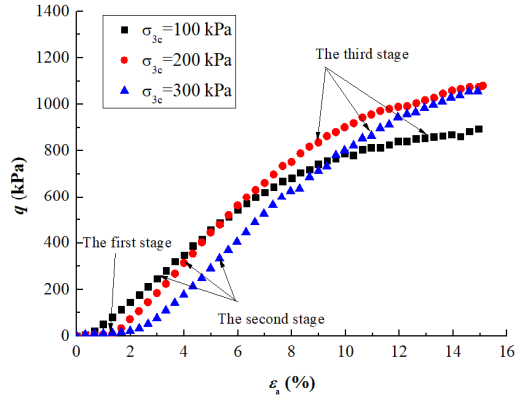

(a)

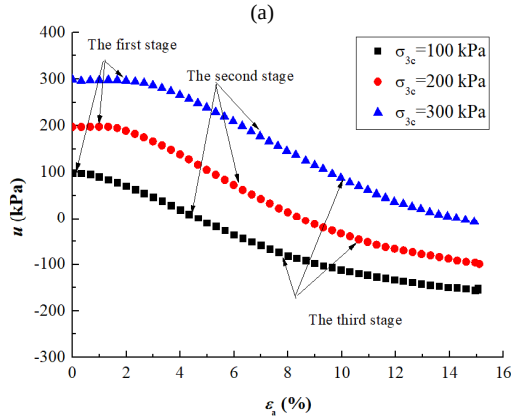

(b)

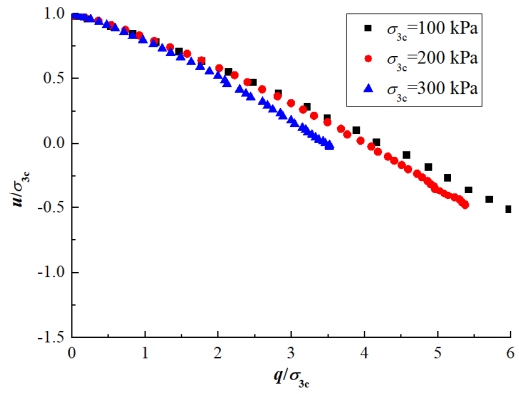

(c)

Fig. 8. Post-liquefaction responses of gravelly soils with different initial effective confining stresses. Variations in (a) the deviatoric stress q; (b) the excess pore water pressure u with axial strain ε_a; and (c) the normalized pore water pressure under different effective confining pressures.

(3) The degree of liquefaction

Monotonic loading tests with different degrees of liquefaction were conducted by changing the number of vibration cycles under the same dynamic loading. Fig. 9 shows the responses of gravelly soils with different degrees of liquefaction at the same initial dry density (ρ_d = 1.8 g/cm^3) and initial effective confining stress (σ_{3c}=100 kPa). The numbers of cycles of soil specimens to obtain F_l values of 1.5, 1.2, 1, 0.9, and 0.8 are 33, 42, 50, 55, and 60, respectively. The results show that the variation in deviatoric stress and the development of excess pore water pressure for the unliquefied specimens are different from those of the liquefied ones. For example, the response of the gravelly soil specimen with F_l = 1.5 is different from those with lower values of F_l Initially, because the specimen is not liquefied, its excess pore water pressure does not accumulate to the level of the effective confining stress. Its shearing behaviour in the monotonic loading test is similar to that of the specimen without previous cyclic loading (Fig. 6). There is only one stage for the stress-strain curve of the unliquefied specimen in which the shear modulus decreases with increasing axial strain and the pore water pressure continuously decreases due to the dilatancy effect. However, the post-liquefaction responses of the liquefied specimens with different degrees of liquefaction are quite similar, including the abovementioned three stages. Meanwhile, the smaller the F_l value, the longer the low strength stage, and the relatively longer maintenance of the pore water pressure level accumulated in the previous cyclic loading. Moreover, at the third stage, the phenomenon that the shearing stiffness begins to weaken lags behind in the specimen with a higher F_l value, and the specimen tends to show a higher ultimate strength if the axial strain is sufficiently large. This shows that a larger initial degree of liquefaction can prolong the process in which the pore water transforms from the contraction state to free and increases the post-liquefaction strength of gravelly soil under static reloading. The action of initial cyclic loading is more likely to form a stronger soil skeleton in the monotonic reloading process, although liquefaction can destroy the initial structure of gravelly soil.

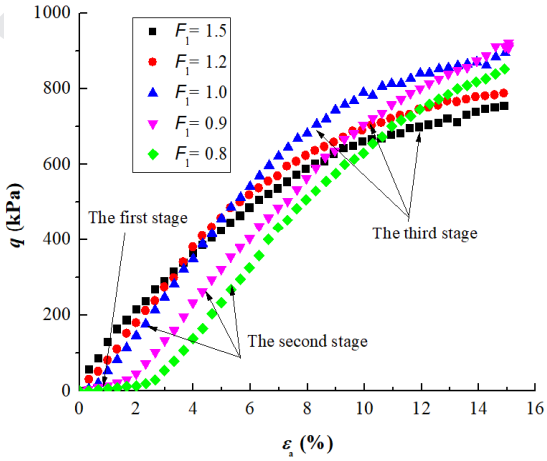

(a)

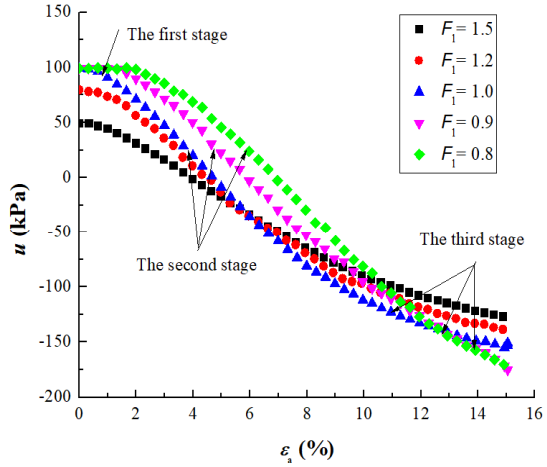

(b)

Fig. 9. Post-liquefaction response of gravelly soil with different degrees of liquefaction. Variation in (a) deviatoric stress q; and (b) excess pore water pressure u with axial strain ε_a.

2.3.3. Comparisons and analysis

Fig. 10 compares the post-liquefaction shearing behaviour between gravelly soil and sand under the same initial conditions (σ_{3c} = 100 kPa, D_r = 50%). It is obvious that the gravelly soil has a higher post-liquefaction shear strength, compared with that of sand. Moreover, the more significant dissipation of excess pore water pressure shows that gravelly soil is more dilatant than sand due to the presence of coarser grains and more irregular particle shapes. For the granular materials, the post-liquefaction shearing behaviours of both gravelly soil and sand have the typical characteristics of three stages, i.e. the low strength stage, the super-linear strength recovery stage, and the sublinear strength recovery stage. The three stages reflect the transition in which the tendency of volume reduction for granular materials accumulated in the liquefaction cycles disappears and the tendency of dilatancy gradually develops during undrained static reloading. In Fig. 6, the fluid-like shear strain ε_{d0} of the low strength stage is relative to the large post-liquefaction deformation. Zhang and Wang (2012) provided an explanation and associated mechanism for large post-liquefaction deformation of sand. They suggested that there is an intrinsic relationship between a volumetric strain component ε_{vc} induced by the change in the mean effective stress and two dilatancy components due to shearing, i.e. a reversible dilatancy component $\varepsilon_{vd,re}$ and an irreversible dilatancy component $\varepsilon_{vd,ir}$. The $\varepsilon_{vd,ir}$ always remains positive, corresponding to volume contraction, and conversely, $\varepsilon_{vd,re}$ always remains negative or equals zero, corresponding to volume expansion. Under undrained conditions, the large post-liquefaction deformation ε_{d0} is triggered in the zero effective confining stress state, and we have

$$\varepsilon_{vc} = -(\varepsilon_{vd,ir} + \varepsilon_{vd,re}) \quad (2)$$

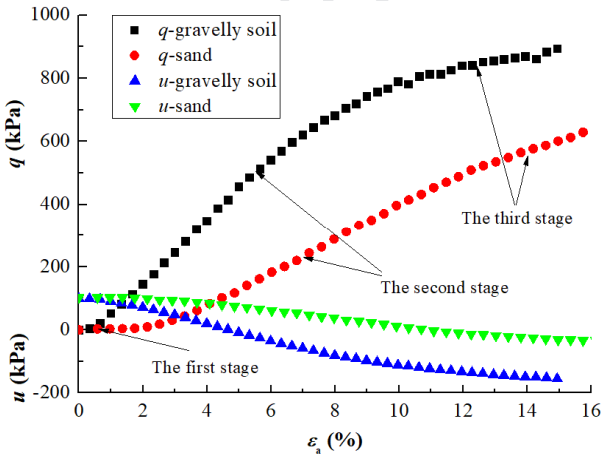

Fig. 10. Comparison of the post-liquefaction shearing behaviours between gravelly soil and sand (D_r = 0.5%).

Since $\varepsilon_{vd,ir}$ is larger than $\varepsilon_{vd,re}$ in the entire liquefaction cyclic shearing, as a consequence, the absolute value of ε_{vc} increases in a swelling manner cycle by cycle. When the effective confining stress decreases from its initial value to zero, ε_{vc} reaches its minimum value. Since $\varepsilon_{vd,ir}$ increases monotonically during the entire loading process, the amplitude of $\varepsilon_{vd,re}$ needs to increase to balance $\varepsilon_{vd,ir}$ and satisfy Eq. (2). Moreover, the generation of sufficiently large $\varepsilon_{vd,re}$ requires a large fluid-like shear strain ε_{d0}. Therefore, at the beginning of the static reloading after liquefaction, the deformation caused by external forces is limited by the deformation compatibility condition of Eq. (1), resulting in generation of fluid-like shear strain ε_{d0} at the low strength stage. Then, due to the reduction in pore water pressure, the zero effective stress state is damaged, which causes termination of the low strength stage. Because of the continuous increase in $\varepsilon_{vd,ir}$ and decrease in $\varepsilon_{vd,re}$ during the reloading process, the absolute value of ε_{vc} becomes increasingly large, which means the gradual development of the tendency of dilatancy. After the pore water wholly transforms to the free state as the axial strain develops, $\varepsilon_{vd,re}$ reaches the minimum value, and the super-linear strength recovery stage ends. Subsequently, because the generation of negative excess pore water causes the increasing effective stress, the tendency of dilatancy in the soil is restrained, and the post-liquefaction shearing behaviour turns into the sublinear strength recovery stage. Compared with those of sand, the low strength stage and the super-linear strength recovery stage of gravelly soil are much shorter, while the sublinear strength recovery stage appears longer. This is because the gravelly soil is prone to generating more significant irreversible shear strain and weaker reversible dilatancy during undrained static reloading.

3. DEM numerical simulations

The DEM provides a way to obtain micro-mechanical information at the grain scale and to understand the macroscopic post-liquefaction shearing behaviour of gravelly soil. In this study, numerical simulations were performed using the DEM code PFC2D (Itasca, 2014).

3.1. Numerical specimen

The size of numerical specimen is 200 mm × 400 mm (width × height), and is composed of 3940 disc particles, as shown in Fig. 11. In the simulation, an assembly consisting of different groups of particle sizes was generated using a compiled C++ subroutine according to the actual particle grades of the gravelly soil specimens, such as 10-20 mm, 5-10 mm, 2-5 mm, and 1-2 mm (particles less than 1 mm were substituted according to the equal quality principle), whose particles met the requirement of random distribution (Bierwisch, 2009). Non-circular particle may be adopted to represent more realistic particle shape and corresponding soil behaviour (Yan, 2011), but it was not used herein to avoid excessive complexity. The linear force-displacement contact model was adopted in the numerical simulations (Gong et al., 2012). The normal contact stiffness k_n of the particle varied according to the radius of the particle R, and the tangential contact stiffness k_s was assumed to be equal to half of k_n (Gu et al., 2013). The microscopic parameters were determined from the results of the biaxial test. The simulation of the biaxial test followed the procedure of the post-liquefaction test, and it was divided into three stages: consolidation, undrained cyclic shearing and monotonic shearing. After particle generation, the assembly was isotropically consolidated to the desired confining stress (100 kPa) by a servo-controlled facility, which was used to increase the wall stress to the target strength by controlling the movement speeds of the walls. The undrained cyclic and monotonic biaxial tests were conducted by keeping the volume constant throughout the shearing process (Chantawarangul, 1993). The cyclic shearing stage was stress-controlled by moving the top and bottom walls at a constant

velocity of 0.1 m/s in opposite directions, and the left and right walls were moved at a constant velocity of 0.05 m/s in opposite directions to maintain the constant volume. The numerical simulations of undrained cyclic triaxial tests were performed using different amplitudes of axial stress until initial liquefaction was reached. Because the PFC program did not include the pore water fluid phase, the pore water pressure of the numerical specimens was obtained by monitoring the variation in the effective stress on the walls (Zhou et al., 2007). The initial liquefaction was considered to occur when the excess pore water pressure reached the effective confining pressure. At this stage, the deviatoric stress in the assembly was displayed at a constant value of zero. Soon after initial liquefaction occurred, the undrained monotonic shearing test was simulated in a strain-controlled manner. The undrained monotonic shearing stage was stopped when the axial strain reached 16%. The axial strain, axial stress, and pore pressure responses were monitored during the biaxial test. A comparison of stress-strain curves from the numerical and experimental results is shown in Fig. 12. Accordingly, the calibrated input parameters of the DEM simulations are shown in Table 2.

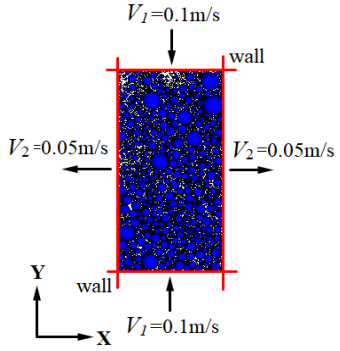

Fig. 11. The numerical model of the specimen.

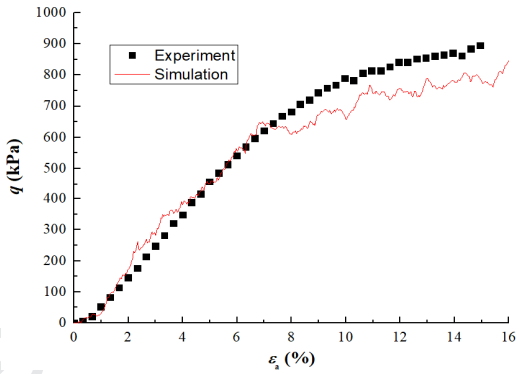

Fig. 12. Comparison of stress-strain curves between the numerical simulation and test.

Table 2.

Parameters in the DEM simulations.

Sample size (mm × mm)	Particle density (kg/m^3)	Porosity	Friction coefficient	Normal contact stiffness (N/m)	Shear contact stiffness (N/m)	Confining stress (kPa)
200 × 400	2760	0.3	0.9	1×10^8	9×10^7	100

3.2. *Simulation results*

3.2.1. *General macro-mechanical features*

Fig. 13 shows the results of DEM numerical simulations of the post-liquefaction undrained response of a typical saturated gravelly soil at an initial effective confining stress of 100 kPa with an initial dry density of 1.8 g/cm^3. The assembly initially deforms with nearly zero stiffness, and its shear capacity is low. With continuous shearing, the stiffness is recovering. The variation in the deviatoric stress is clearly observed in the numerical simulation, which is similar to that in the physical test. Moreover, the three stages (low strength stage, super-linear strength recovery stage and sublinear strength recovery stage) of the post-liquefaction stress-strain curve of gravelly soil can also be distinguished, which is also consistent with the experimental observations (see Fig. 6).

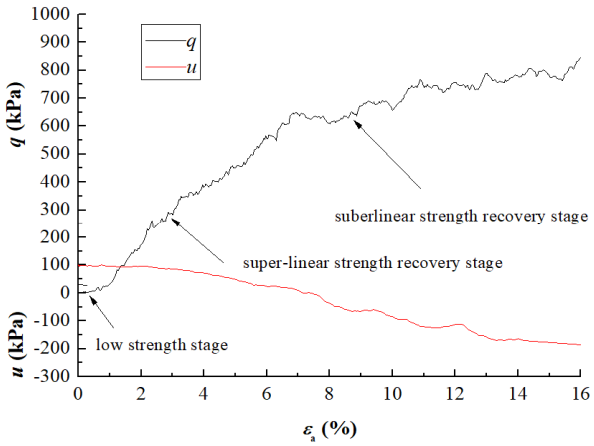

Fig. 13. The numerical biaxial test results of post-liquefaction responses of gravelly soil.

3.2.2. *Evolution of the average coordination number*

The coordination number is an important microscopic parameter affecting the mechanical behaviour of granular materials (Thornton, 2000; Gu et al., 2014), which refers to as the number of particles in contact with a given particle. One particle can contact one or several neighbouring particles. Fig. 14 shows the variation in the average coordination number with the axial strain at a confining stress of 100

kPa and initial dry density of 1.8 g/cm^3. The average coordination number is small (nearly zero) at the beginning ($\varepsilon_a \leq 1\%$). There is very weak or no contact between particles. When the axial shear strain increases from approximately 2% to 4%, the average coordination number rises sharply to above 3, which is a threshold value describing the stable and unstable soil behaviours based on simple analysis (Rothenburg and Kruyt, 2004). It shows that there is an intense rearrangement of particles taking place during the process, and the assembly quickly reaches a stable state (Edwards, 1998). Because of the larger gravel particles, the dilatancy trend of the soil skeleton is stronger. The initial contraction state of the pore water at liquefaction is rapidly released and then the reduction in pore water pressure is induced. Accordingly, the external load quickly transfers the pressure from the pore water to the soil skeleton, giving rise to the intense rearrangement of the particle system. When the axial shear strain is above 4%, the average coordination number increases steadily during the monotonic loading, which means that the drastic adjustment of particles has already been completed and a stable packing has developed. However, subtle local adjustments of the granular system continue with increasing effective stress.

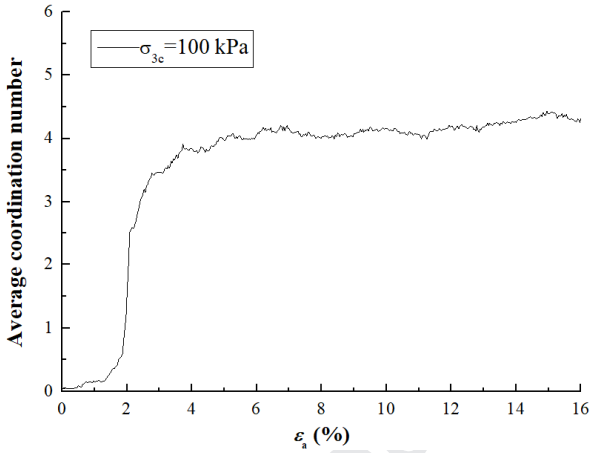

Fig. 14. Evolution of the average coordination number with the axial strain ε_a in the DEM simulation.

3.2.3. Evolution of the fabric and force chain

Fabric, which is usually defined as the spatial arrangement of particles (Ibrahim and Kagawa, 1991), plays a key role in controlling the microscopic behaviour of granular materials. The distribution of the contact normals is an important characteristic of fabric and is an indicator that reflects material anisotropy. Fig. 15 shows the orientation distributions of contact normals for the numerical specimen at different axial strains during monotonic reloading. The anisotropy evolution of the specimen under monotonic shearing can be observed clearly. As shown in Fig. 15, the contact normal is nearly chaotic after liquefaction at axial strain ε_a = 0%, and the state does not change significantly within a small range of axial strain (less than 1%). However, we can still observe the gradual increase in the variety of contact normal angles (see Fig. 12a,b). This means that the interaction of the particles is weak, and few contacts exist after liquefaction of the gravelly soil. At the low strength stage, there are a growing number of contacts. Subsequently, when the axial strain increases to approximately 4% from 2%, the contact normal rapidly shows an orientation distribution, which is mainly concentrated at the orientation of 90° and 270°. This indicates that a drastic rearrangement (e.g. rolling, rotating, and slipping of particles) of the assembly occurs during the process. With increasing axial strain, although the distribution of contact normals has some subtle changes, the angles of orientation are nearly unchanged (90° and 270°). The orientation is opposite to the shearing direction of the external load. A clear anisotropic characteristic of the contact normal is formed, which means that the drastic rearrangement of particles has already been completed, but only the continuous local subtle adjustments of the granular system with the axial strain. There is a good relationship between the evolution of contact normal distributions and the average coordination number.

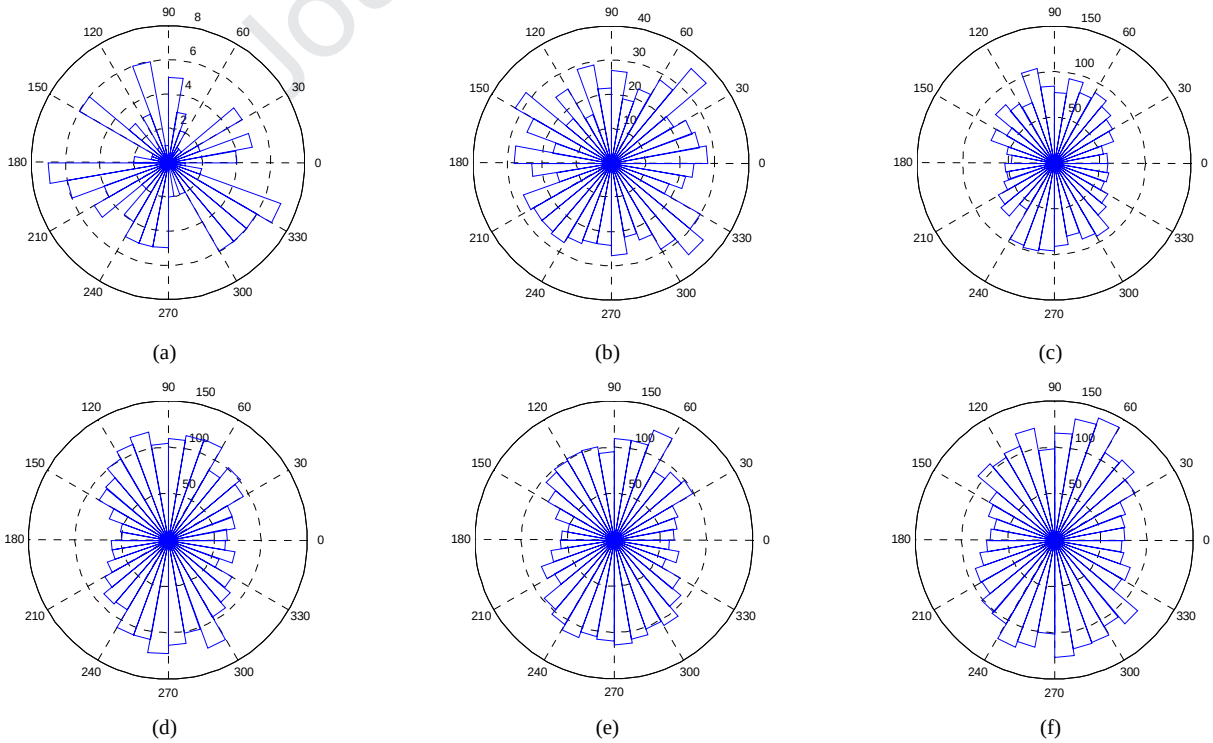

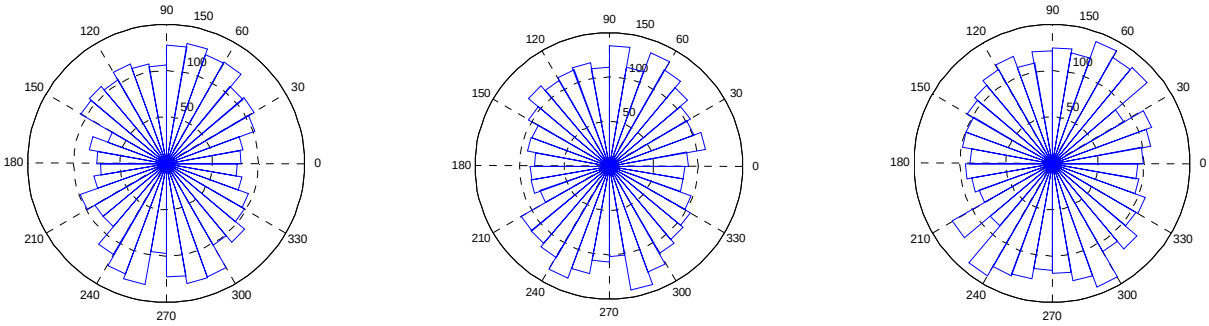

(g) (h) (i)

Fig. 15. The orientation distributions of contact normals for the gravelly soil specimens at different axial strains under monotonic reloading: (a) ε_a = 0%; (b) ε_a = 2%; (c) ε_a = 4%; (d) ε_a = 6%; (e) ε_a = 8%; (f) ε_a = 10%; (g) ε_a = 12%; (h) ε_a = 14%; and (i) ε_a = 16%.

3.2.4. Evolution of the force chain

The force chain can also be used to reveal the post-liquefaction deformation behaviour of saturated gravelly soil from the micro-mechanism point of view. Fig. 16 shows the internal force-chain distribution evolution for the initially liquefied specimen under monotonic reloading (CForce is the contact force between the particles). In the beginning, the force chain network of the specimen is destroyed by liquefaction (Fig. 16a). With increasing axial strain (less than 2%), the force chains quickly develop. The shear resistance of the specimen starts to recover. In particular, the force chain networks (consisting of strong and weak force chains) are firstly formed at the top and bottom of the specimen (Fig. 16b). When the axial strain reaches 4%, the force chain networks at the top and bottom almost develop symmetrically and run through the specimen rapidly, which is centralised along the central axis. A dumbbell-shaped network structure composed of strong force chains is initially formed (see Fig. 16c), suggesting the formation of a backbone of force chains and stable packing. The corresponding phase is just at the moment when the contact normal rapidly forms the orientation distribution (mainly concentrated on 90° and 270°). Subsequently, as the external load increases, more backbone force chains begin to form (see Fig. 16d). The backbone force chains are approximately aligned in the vertical direction to counterbalance the external load. The wide range of drastic rearrangements (particle movement of rolling or rotating) of assembly has nearly been completed, with the formation of backbone force chains in a relatively fixed orientation. Then, the number of backbone force chains increases gradually, and the whole force chain network forms eventually (see Fig. 16e to f). The completion of the abovementioned micro-processes suggests that the macro phenomenon — the super-linear strength recovery stage — is finished. In the macroscopically sublinear strength recovery stage, with further shearing, the configuration of the whole force chain network and the number of backbone force chains have almost no significant change, but the whole number of force chains increases (see Fig. 16 h,i). This shows that the drastic rearrangement of the granular system stops, but the local subtle adjustments continue until the shearing test is terminated.

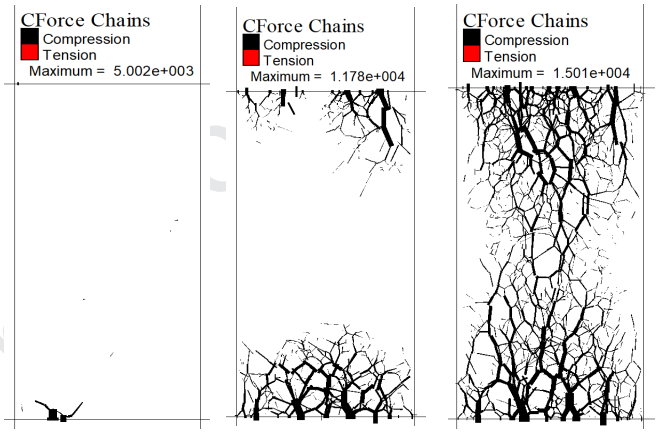

(a) (b) (c)

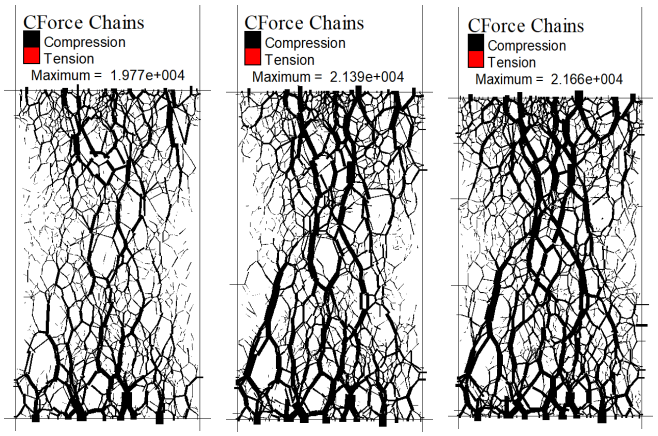

(d) (e) (f)

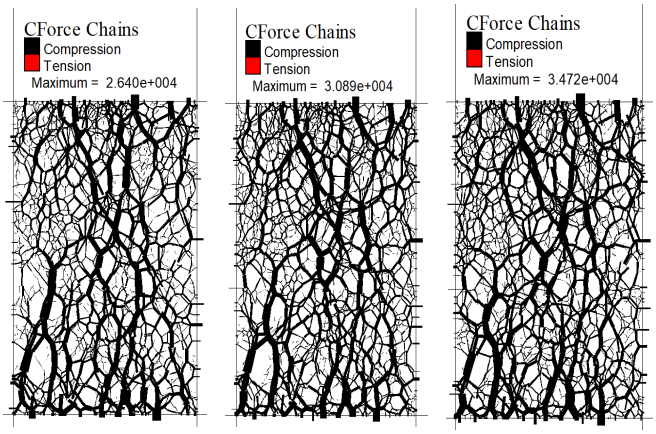

(g) (h) (i)

Fig. 16. The force chain evolution of liquefied gravelly soil specimens at different axial strains under monotonic loading: (a) ε_a = 0%; (b) ε_a = 2%; (c) ε_a = 4%; (d) ε_a = 6%; (e) ε_a = 8%; (f) ε_a = 10%; (g) ε_a = 12%; (h) ε_a = 14%; and (i) ε_a = 16% (the thickness of the line represents the magnitude of the contact force).

From the above results, there is a good correspondence between the evolution of micro-parameters and macro-mechanical properties. Variations in the average coordination number, evolution of the contact normal distribution and reconstruction of the backbone of force chains all reveal the micro-mechanism of post-liquefaction shearing behaviour of saturated gravelly soil from different perspectives.

4. Conclusions

In this study, undrained static-dynamic triaxial tests and preliminary numerical simulations were conducted to investigate the post-liquefaction shearing behaviour of saturated gravelly soil. The effects of the initial dry density, initial confining stress, and degree of liquefaction on the stress-strain behaviours, the evolution of excess pore water pressure and the micro-parameters of the post-liquefaction deformation were analysed. The major conclusions are drawn as follows:

(1) The shearing behaviour of gravelly soil after liquefaction is significantly different from that of the general saturated gravelly soil in monotonic reloading. Its stress-strain curve can be divided into three stages: low strength stage, super-linear strength recovery stage and sublinear strength recovery stage. Due to the coarser grains and more irregular particle shapes, gravelly soil is prone to generating more significant irreversible strain and weaker reversible dilatancy during the undrained static reloading, which leads to shorter low strength and super-linear strength recovery stages but longer sublinear strength recovery stage than those of sand.

(2) The post-liquefaction shearing behaviour of gravelly soil distinctly depends on the initial state and prior dynamic stress history. The initial dry density, confining stress and degree of liquefaction have different effects on the behaviour of gravelly soil after liquefaction, which leads to different responses of excess pore water pressure and performances of the three stages of the stress-strain curves.

(3) The micro-structural parameters greatly affect the macroscopic post-liquefaction shearing behaviour of saturated gravelly soil during monotonic reloading. The average coordination number sharply increases, and the contact normal shows an obvious orientation distribution and the destroyed backbone of force chains reconstructs, which significantly reflect the interior interaction process and effect in the granular particle system during the three stages of the macro-mechanical behaviour of gravelly soil.

Declaration of Competing Interest

The authors wish to confirm that there are no known conflicts of interest associated with this publication and there has been no significant financial support for this work that could have influenced its outcome.

Acknowledgments

The work presented in this paper is financially supported by the National Natural Science Foundation of China (Grant Nos. 51979269, 51779017, and 41702348). The authors are also very grateful to the reviewers for their valuable comments and suggestions.

List of symbols

G_s	Specific gravity
e	Void ratio
e_{max}	Maximum void ratio
e_{min}	Minimum void ratio
ρ_d	Dry density
σ_d	Single axial stress amplitude
σ_c	Effective confining stress
σ_{3c}	Initial effective confining stress
F_l	Anti-liquefaction safety factor
n	Number of vibration cycles at initial liquefaction failure
m	Total number of vibration cycles under the same cyclic shear stress ratio
ε_a	Axial strain
ε_{d0}	Axial strain of the low strength stage
ε_{d1}	Axial strain of the dividing point between the low strength stage and the super-linear strength recovery stage
q	Deviatoric stress
q_0	Deviatoric stress corresponding to ε_{d0}
q_1	Deviatoric stress corresponding to ε_{d1}
u	Static excess pore water pressure
u_d	Dynamic excess pore water pressure
$\Delta\sigma_3$	The increase in confining stress applied to the specimen
Δu	The resulting change in pore water pressure

References

Baneriee NG, Seed HB, Chan CK. Cyclic behavior of dense coarse-grained materials in relation to dams. No. UCB /EERC(79/13); 1979.

Been K, Jefferies MG. A state parameter for sands. Géotechnique 1985;35(2):99–112.

Bierwisch C. Numerical simulations of granular flow and filling (PhD Thesis). Freiburg, Germany: University of Freiburg; 2009.

Cao ZZ, Hou L, Xu H, Yuan XM. Distribution and characteristics of gravelly soil liquefaction in the Wenchuan M_s 8.0 earthquake. Earthquake Engineering and Engineering Vibration 2010;9:167–75.

Cao ZZ, Youd TL, Yuan XM. Gravelly soils that liquefied during 2008 Wenchuan, China earthquake, M_s=8.0. Soil Dynamics and Earthquake Engineering 2011;31(8):1132–43.

Cao ZZ, Youd TL, Yuan XM. Chinese dynamic penetration test for liquefaction evaluation in gravelly soils. Journal of Geotechnical and Geoenvironmental Engineering 2013;139(8):1320–33.

Chang WJ, Chang CW, Zeng JK. Liquefaction characteristics of gap-graded gravelly soils in K_0 condition. Soil Dynamics and Earthquake Engineering 2014;56:74–85.

Chantawarangul K. Numerical simulations of three-dimensional granular assemblies. PhD Thesis. Waterloo, Canada: University of Waterloo; 1993.

Chen LW, Yuan XM, Cao ZZ, Hou LQ, Sun R, Dong L, Wang WM, Meng FC, Chen HJ. Liquefaction macrophenomena in the great Wenchuan earthquake. Earthquake Engineering and Engineering Vibration, 2009;8(2):219–29.

Cubrinovski M, Henderson D, Bradley BA. Liquefaction impacts in residential areas in the 2010-2011 Christchurch earthquakes. In: Proceedings of the International Symposium on Engineering Lessons Learned from the Giant Earthquake. Canterbury, New Zealand: University of Canterbury; 2012. p. 811–24.

Edwards SF. The equations of stress in a granular material. Physica A: Statistical Mechanics and its Applications 1998;249(1):226–31.

Evans MD, Zhou S. Liquefaction behavior of sand-gravel composites. Journal of Geotechnical Engineering 1995;121(3):287–98.

Fukutake K, Ohtsuki A, Sato M, Shamoto Y. Analysis of saturated dense sand-structure system and comparison with results from shaking table test. Earthquake Engineering Structural Dynamics 1990;19(7):977–92.

Gong GB, Thornton C, Andrew HCC. DEM simulations of undrained triaxial behavior of granular material. Journal of Engineering Mechanics 2012;138:560–66.

Gu XQ, Yang J. A discrete element analysis of elastic properties of granular materials. Granular Matter 2013;15(2): 139–47.

Gu XQ, Huang MS, Qian JG. DEM investigation on the evolution of microstructure in granular soils under shearing. Granular Matter 2014;16:91–106.

Hamada M, Rourke TDO. Large ground deformations and their effects on lifelines: 1964 Niigata earthquake. Case studies of liquefaction and lifelines performance during past earthquake. Technical Report NCEER-92-0001, Vol. 1; 1992.

Ibrahim AA, Kagawa T. Microscopic measurement of sand fabric from cyclic tests causing liquefaction. Geotechnical Testing Journal 1991;14(4):371–82.

Ishikawa A, Zhou YG, Shamoto Y, Mano H, Chen YM, Ling DS. Observation of post-liquefaction progressive failure of shallow foundation in centrifuge model tests. Soils and Foundations 2015;55(6):1501–11.

Itasca. Particle flow code of two-dimensional programs (PFC2D 6.0). Minneapolies: Itasca Consulting Group Inc, 2014.

Kokusho T, Tanaka Y, Kudo K, Kawai T. Liquefaction case study of volcanic gravel layer during 1993 Hokkaido-Nansei-Oki earthquake. In: Proceedings of the 3rd International Conference on Recent Advances in Geotechnical Earthquake Engineering and Soil Dynamics; 1995. p. 235–42.

Kokusho T, Hara T, Hiraoka R. Undrained shear strength of granular soils with different particle gradations. Journal of Geotechnical and Geoenvironmental Engineering 2004;130(6):621–9.

Lin PS, Chang CW, Chang WJ. Characterization of liquefaction resistance in gravelly soil: Large hammer penetration test and shear wave velocity approach. Soil Dynamics and Earthquake Engineering 2004;24(9-10):675–87.

Pan H, Chen GX, Sun T, Liu HL. Behaviour of large post-liquefaction deformation in saturated sand−gravel composites. Journal of Central South University 2012;19:547–52.

Rothenburg L, Kruyt NP. Critical state and evolution of coordination number in simulated granular materials. International Journal of Solids and Structures 2004;41:5763–74.

Seed HB, Lee KL. Liquefaction of saturated sands during cyclic loading. Journal of Soil Mechanics & Foundations Division 1966;92(6):105–34.

Shamoto Y, Zhang JM, Goto S. Mechanisms of large post-liquefaction deformation in saturated sand. Soils and Foundations 1997;37(2):71–80.

Tanaka Y, Kokusho T, Yoshida Y, Kudo K. A method to evaluate membrane compliance and system compliance in undrained cyclic shear tests. Soils and Foundations 1991;31(3):30-42.

Thornton C. Numerical simulations of deviatoric shear deformation of granular media. Géotechnique 2000;50(1):43–53.

Tohno I, Shamoto Y. Liquefaction damage to the ground during the 1983 Nihonkai-Chubu Earthquake in Akita prefecture. Natural Disaster Science 1985;7(2):67–93.

Tokimatsu K, Nakamura K. A simplified correction for membrane compliance in liquefaction tests. Soils and Foundations 1987;27(4):111–22.

Tokimatsu K, Kojima H, Kuwayama S, Abe A, Midorikawa S. Liquefaction-induced damage to buildings in 1990 Luzon earthquake. Journal of Geotechnical Engineering 1994;120(2):290–307.

Hou LQ, Li AF, Qiu ZM. Characteristics of gravelly soil liquefaction in Wenchuan earthquake. Applied Mechanics and Material 2011:90-93:1498-502.

Wang YL, Cheng ZL, Wang Y. Effects of liquefaction-induced lateral ground deformation on pile foundations. Journal of Central South University 2013;20:2510–8.

Wang YL, Wang Y. Pore characteristics of sand-gravel mixtures based on the intergranular state parameters. Electronic Journal of Geotechnical Engineering 2017a;22(2):531–9.

Wang Y, Wang YL. Liquefaction characteristics of gravelly soil under cyclic loading with constant strain amplitude by experimental and numerical investigations. Soil Dynamics and Earthquake Engineering 2017b;92:388–96. Wong RT, Seed HB, Chan CK. Cyclic loading liquefaction of gravelly soils. Journal of the Geotechnical Engineering Division 1975;101(6):561–83.

Xu B, Kong XJ, Zou DG, Lou SL. Laboratory study on behaviour of static properties of saturated sand-gravel after liquefaction. Chinese Journal of Geotechnical Engineering 2007;29(1):103–6 (in Chinese).

Yan WM. Particle elongation and deposition effect to macroscopic and microscopic responses of numerical direct shear tests. Geotechnical Testing Journal 2011;34(3):238–49.

Yasuda S, Yoshida N, Masuda T, Nagase H, Kiku H. Stress-Strain Relationships of Sand after Liquefaction In: Proceedings of the International Conferences on Recent Advances in Geotechnical Earthquake Engineering and Soil Dynamics; 1995. p. 295–8.

Yasuda S, Harada K, Ishikawa K, Kanemaru Y. Characteristics of liquefaction in Tokyo Bay area by the 2011 Great East Japan Earthquake. Soils and Foundations 2012;52(5):793–810.

Yoshida N, Watanabe H, Yasuda S, Sergio MC. Liquefaction-induced ground failure and related damage to structures during 1991 Telire-Limon, Costa Rica, earthquake. In: Proceedings of the 4th Japan-U.S. Workshop on Earthquake Resistant Design of Lifeline Facilities and Countermeasures for Soil Liquefaction; 1992. p. 37–52.

Zhang JM, Wang G. Large post-liquefaction deformation of sand, part I: Physical mechanism, constitutive description and numerical algorithm. Acta Geotechnica 2012;7:69–113.

Zhou J, Shi DD, Jia MC. Micro-mechanical simulation of liquefaction behavior of saturated sand under cyclic loading. Journal of Hydraulic Engineering 2007;38(6):697–703.

Dr. Yong Wang is Associate Professor at Institute of Rock and Soil Mechanics, Chinese Academy of Sciences, China, where he received his PhD degree in engineering mechanics in 2009.

He is a member of Geotechnical Testing Committee, Chinese Institution of Soil Mechanics and Geotechnical Engineering, China Civil Engineering Society (2014-present); member of Commission for Marine Engineering Geology, International Association for Engineering Geology and the Environment (2019-present). His research interests are in soil mechanics testing and multiscale soil mechanical behaviours with particular focus on granular soils, sand, and gravelly soil liquefaction, marine gas-bearing sediments, and unsaturated soil as well as numerical simulation analysis.

Highlights

1. This work investigated the post-liquefaction shearing behavior of gravelly soil based on the static-dynamic multi-functional triaxial apparatus. The macroscopic stress-strain response of gravelly soil after liquefaction was divided into three typical stages.
2. The influencing factors of the dry density, initial confining stress and degree of liquefaction on the post-liquefaction shearing behavior of gravelly soil were studied and analyzed.
3. Based on DEM simulations on the monotonic reloading test after liquefaction of saturated gravelly soil, the interior micro-mechanisms and interaction evolution process in the granular particle system were revealed and discussed in the three different stages of macro-deformation behavior.

Declaration of interests

☒ The authors declare that they have no known competing financial interests or personal relationships that could have appeared to influence the work reported in this paper.

☐The authors declare the following financial interests/personal relationships which may be considered as potential competing interests: